Dalton Transactions

Cite this: *Dalton Trans.*, 2012, **41**, 6764

www.rsc.org/dalton

PAPER

Copper(II) complexes of bis(amino amide) ligands: effect of changes in the amino acid residue†

Inés Martí, Armando Ferrer,‡ Jorge Escorihuela, M. Isabel Burguete and Santiago V. Luis*

Received 20th December 2011, Accepted 23rd March 2012
DOI: 10.1039/c2dt12459a

A family of ligands derived from bis(amino amides) containing aliphatic spacers has been prepared, and their protonation and stability constants for the formation of Cu^{2+} complexes have been determined potentiometrically. Important differences are associated to both the length of the aliphatic spacer and the nature of the side chains derived from the amino acid. In general, ligands containing aliphatic side chains display higher basicities as well as stability constants with Cu^{2+}. In the same way, basicities and stability constants tend to increase when decreasing the steric hindrance caused by the corresponding side-chain. FT-IR, UV-vis and ESI-MS were used for analyzing the complex species detected in the speciation diagram. UV-vis studies showed the presence of different coordination environments for the copper(II) complexes. Complexes with different stoichiometries can be formed in some instances. This was clearly highlighted with the help of ESI-MS experiments.

Introduction

The coordination of metal cations with tetradentate ligands containing four nitrogen electron donors is common to many coenzymes and catalytic models.[1] Metalloenzymes usually contain metal ions bound to an amino group of a specific amino acid residue of a peptide or directly to the amide group – carbonyl or nitrogen – offering different coordination environments.[2] Thus, a proper design of small molecules with suitable structural and functional characteristics could be important for future catalytic, biomimetic and recognition studies. In this regard, the design and synthesis of ligands functionalized to achieve metal complexation in a biomimetic approach is a challenge of current interest.[3] The inclusion of amino acid residues in the structure is one of the most obvious strategies to provide coordination environments of the metal ions similar to those found in metalloproteins.[4] On the other hand, the presence of chirality derived from the amino acid subunits allows the potential application of those derivatives in enantioselective catalysis to be considered.[5]

In this context, C_2 symmetric bis(amino amide) ligands appear as promising ligands for several reasons: (i) they can be easily prepared by standard and simple synthetic protocols; (ii) they contain two kinds of nitrogen atoms, with different coordination capabilities, connected through a chiral backbone; (iii) their properties can be easily tuned by the selection of the appropriate R-carbon substituents (R, Chart 1) and the spacer and (iv) they can form robust metal complexes with transition metals. Bis(amino amides) have been used as building blocks for the construction of macrocyclic structures whose macrocyclization processes have been based on the preorganization induced by conformational elements,[6] configurational factors,[7] or through the use of anionic templates.[8] Some of those systems are able to display interesting features, behaving as organogelators,[9] acting as '*in vivo*' fluorescent pH probes,[10] as selective receptors for substrates of biological relevance,[11] as minimalistic molecular machines,[12] as ligands for the preparation of enantioselective catalysts or as chiral solvating agents.[13] On the other hand, the self-assembly of this kind of compound in the solid state has also allowed the observation of some remarkable crystalline structures and nano-assembled morphologies with relevance for the

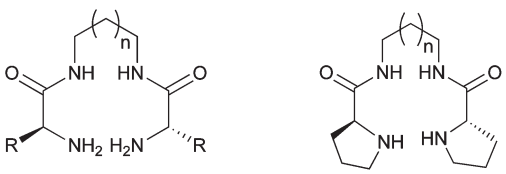

1a R=CH_2Ph PheA(n+2)
1b R=Ph PhglyA(n+2)
1c R=H GlyA(n+2)
1d R=CH_3 AlaA(n+2)

2a ProA(n+2)

Chart 1 The bis(amino amides) studied in this work.

Departamento de Química Inorgánica y Orgánica, Universitat Jaume I, Avda. Sos Baynat s/n., 12071 Castellón, Spain. E-mail: luiss@qio.uji.es; Fax: +34 964 72 8214; Tel: +964728239

†Electronic supplementary information (ESI) available: Species distribution curves for the different protonated forms of the ligands and for their corresponding copper(II) complexes (S1 and S2). UV-vis Spectra (S3), Mass Spectra (S4) and experimental data for ligand AlaA3. CCDC 801764 (CuPhglyA2) and 829491 (CuPheA3). For ESI and crystallographic data in CIF or other electronic format see DOI: 10.1039/c2dt12459a

‡Permanent address: Departamento de Química, Facultad de Ciencias Naturales, Universidad de Oriente, Avda. Patricio Lumumba s/n., 90500 Santiago de Cuba, Cuba. E-mail: aferrer@cnt.uo.edu.cu.

understanding of structural parameters in proteins and related peptidic systems.[14]

Recently, we have studied the coordination ability of some C_2 symmetrical bis(amino amides) derived from valine towards Cu(II) and Zn(II) ions.[15] Here, we present the study of the acid–base properties of some related bis(amino amide) ligands derived from other amino acids, as well as the analysis of their binding ability towards a cation playing a key role in bioinorganic chemistry such as Cu^{2+}. The main structural variation considered, besides the length of the spacer, has been the selection of the starting amino acids, in order to analyze the effect of the changes in the side chain on the coordination capabilities of the corresponding bis(amino amides). Thus, compounds derived from glycine, alanine, proline, phenylalanine and the non-natural phenylglicine amino acids have been studied.

Results and discussion

The general structure of the ligands considered is displayed in Chart 1. Open-chain bis(amino amides) derived from amino acids can be easily prepared starting from the corresponding *N*-Cbz protected amino acid through the initial formation of their activated *N*-hydroxysuccinimide esters, coupling with a variety of diamines and final *N*-deprotection, following previously reported procedures.[6b]

For the naming of the compounds in Chart 1, the acronym aaAN has been used for the sake of simplicity. In it, aa refers to the constituent amino acid (*i.e.* PheA*N* for phenylalanine derivatives), while A*N* indicates the length of the aliphatic central spacer, with $N = (n + 2)$ (*i.e.*: PheA6 for a phenyl alanine derivative with a central spacer having six methylene groups).

Acid–base properties

The study of the acid–base properties of the ligands is essential for a proper understanding of the coordination ability of nitrogenated compounds.[4] Initially, bis(amino amide) ligands derived from phenylalanine with spacers from 2 to 6 carbon atoms were selected to study their acid–base properties by the use of pH-metric titrations.[16] This allowed the effect of the length of the methylenic spacer between the two amino amide subunits to be investigated. All the titrations were carried out as has been fully described in the experimental section, at 298.1 ± 0.1 K using 0.1 M NaCl to maintain a constant ionic strength. The stepwise basicity constants for the protonation of ligands derived from phenylalanine obtained in this way are presented in Table 1.

All the compounds display two stepwise basicity constants within the pH range of the study (2–12). Both of them correspond to the protonation of the primary amino groups. Although there is a very slight increase in basicity following the increase in the number of methylene groups in the bridge separating the amide groups, the most noticeable aspect is, however, the resemblance of the stepwise basicity constants for all these compounds. The separation between the positive charges seems to be high enough to make the basicity of all these compounds very close. As an example, the species distribution diagram corresponding to the protonation of PheA3 (**1a**, $n = 1$) is given in Fig. 1. The diagram shows how the L species are predominant at basic pH values while the H_2L species are the major species for the acid pH range. The HL species are only significant at pH values slightly above neutrality. Very similar distribution diagrams for the protonated species were obtained for all ligands (see ESI†). The values of the stepwise protonation constants are slightly lower than the ones previously found for the analogous valine derivatives.[15]

The protonation process can also be monitored by ^{1}H NMR spectroscopy.[17] Upon protonation of polyamine compounds, the hydrogen nuclei attached to the carbon in the α-position to the nitrogen atom bearing the proton are those exhibiting the largest downfield changes in their chemical shift.[18] Therefore, we recorded the ^{1}H NMR spectra of the ligands *versus* pD. For all the cases, the protonation of the amino groups is accompanied, as could be expected, by a significant downfield shift of the proton attached to the stereogenic carbon atom. The protonation also has a minor effect on the shift of some of the protons located at the spacer. This can be observed in Fig. 2, for PheA3. Both the protons labelled as H_D, at two-bond distance from the primary nitrogens, and the protons labelled as H_C, at the α-carbon, experience their maximum downfield shift at very acidic pH ($\Delta\delta$ = 0.37 ppm and $\Delta\delta$ = 0.58 ppm, respectively). This corresponds to the occurrence of the full protonation of the two primary amino groups of the ligand (H_2L formation). Similar trends were observed for ligands with longer hydrocarbon chains between the coordination sites.

Molecular modelling suggests the predominance of very different conformations for the non-protonated and protonated species as a function of the side chain.[15] In this regard, we studied, for each considered amino acid, the protonation of the

Table 1 Logarithms of the cumulative and stepwise basicity constants determined in 0.1 M NaCl at 298.1 ± 0.1 K

Reaction[ac]	PheA2	PheA3	PheA4	PheA5	PheA6
H + L ⇌ HL	7.57(1)[b]	7.64(1)	7.73(3)	7.66(4)	7.69(4)
2H + L ⇌ H_2L	14.27(1)	14.47(1)	14.56(2)	14.71(3)	14.71(3)
H + HL ⇌ H_2L	6.70(1)	6.83(1)	6.83(3)	7.05(4)	7.02(4)

[a] Charges omitted for clarity. [b] Values in parentheses are the standard deviations in the last significant figure. [c] Determined in 0.1 M NaCl using 50 mL of a 2 mM solution of the ligand.

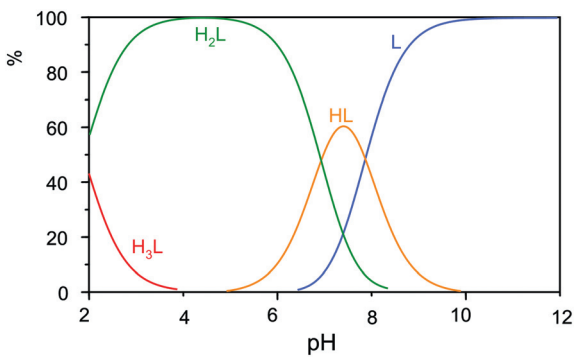

Fig. 1 Distribution diagram for the protonated species of PheA3 in 0.1 M NaCl at 298.1 K.

ligands with the shortest (n = 0) and longest aliphatic spacers (n = 4). The corresponding protonation constants were obtained from the analysis of potentiometric titrations at 298.1 ± 0.1 K in 0.1 M NaCl, and their values are included in Table 2. The values previously obtained for the related valine derived bis(amino amides) have also been included for comparison.[15]

As can be seen in Table 2, there is, in all cases, a very slight increase in basicity following the increase in the number of methylene groups in the bridge separating the amide groups, as had been noticed for Phe. The ligand AlaA3 was also studied (see ESI†) to confirm that intermediate lengths follow similar trends as observed for Val and Phe. When the nature of the side chain is considered, it can be observed that basicity constants are always lower for derivatives containing aromatic side chains (Phe and Phgly derivatives). The effect is bigger for phenylalanine than for phenylglicine and decreases when going from A2 to A6. The most remarkable aspect is, however, the high values obtained for proline derivatives. Additionally, the compounds derived from the amino acids with the smaller side chains (Gly, Ala) present slightly higher protonation constants than those with larger side chains (*i.e.* derived from Val, Phe or Phgly). This can be associated to solvation effects being more favourable for the compounds with smaller hydrophobic side chains. The p*K*a values for simple amino acids seem to follow a similar trend, although the differences are higher for the pseudopeptides studied here. Thus, Pro is the most basic of the amino acids considered in this work (10.6), followed by Ala (9.69) and Gly (9.6), while Phe is less basic (9.16).[19] The corresponding distribution diagrams have been included in the ESI† and show observable differences reflecting the changes in the values of the protonation constants. Thus, for example, when Pro derivatives are considered, the H_2L species predominates from *ca.* pH 8 and HL is the major species at around pH 9, while for PhglyA2 the H_2L species only predominates from pH values below 5.5 (6.5 for PhglyA6). In the case of GlyA2, the obtained basicity constants are in good agreement with those previously described.[20]

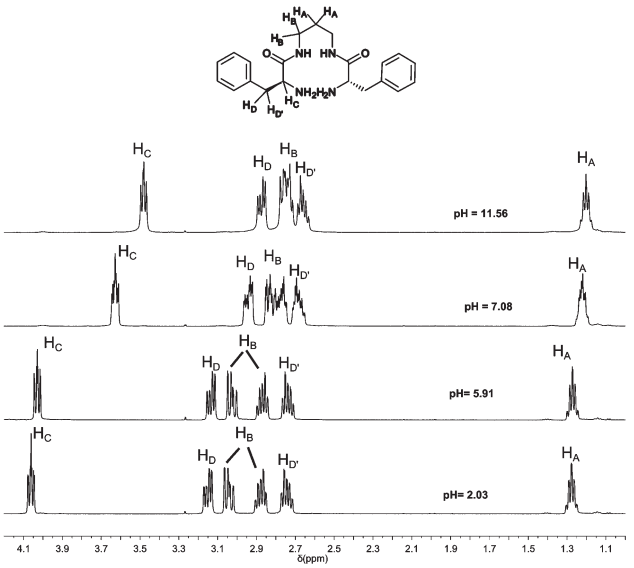

Fig. 2 Variation of the chemical shift of the ^{1}H signals with pD for the ligand PheA3.

Interaction with Cu^{2+}

Because of the interest of developing copper(II)-containing model systems for metalloproteins, and taking into account our previous experience in this field, the copper(II) complexes of the new ligands were investigated to explore their coordination chemistry.[21] The equimolecular reaction of the bis(amino amide) ligands and Cu^{2+} chloride in a saturated methanolic solution of KOH, to ensure the complete deprotonation of the ligand, afforded bright colored solids. Upon complexation, the carbonyl frequency (FT-IR) shifts from 1629.5 cm^{-1} in the free ligands to 1571.7 cm^{-1} in the copper(II) complexes (see Fig. 3). This indicates the participation of the deprotonated amide group in the coordination to Cu^{2+}, in agreement with the data obtained by potentiometry and for related systems.[22]

The interaction of Cu^{2+} and the new ligands was systematically studied by potentiometric titrations in aqueous solution over the 2–12 pH range. The stability constants for the formation of Cu^{2+} complexes have been determined in water using 0.1 M NaCl to maintain a constant ionic strength and at 298.1 ± 0.1 K. Initially, we determined the stability constants for the family of ligands derived from phenylalanine in order to investigate the effect of the methylenic spacer. The results obtained are presented in Table 3 and in Fig. 4. It can be observed that the length of the central spacer is critical for determining the complex speciation obtained. For the shorter spacers (A2 and A3) only two complex species (monodeprotonated and bisdeprotonated) are detected. The non-deprotonated $[CuL]^{2+}$ species is only detected for the ligands with the larger spacers at pH values around 6. The monoprotonated $[CuHL]^{3+}$ species is only observed for PheA4. On the other hand, the relative importance of the $[CuH_{-1}L]^{+}$ species is very different along this series. It is predominant around pH 6 for PheA2, but it is a very minor species for PheA3. The importance of this species grows again for longer

Table 2 Logarithms of the cumulative and stepwise basicity constants of compounds determined in 0.1 M NaCl at 298.1 ± 0.1 K

Reaction[ac]	AlaA2	AlaA6	GlyA2	GlyA6	PhglyA2	PhglyA6	ProA2	ProA6	ValA2[d]	ValA6[d]
$H + L \rightleftharpoons HL$	8.30(1)[b]	8.37(5)	8.21(5)	8.70(4)	7.49(10)	7.64(5)	9.04 (1)	10.16(7)	7.94(1)	8.16(1)
$2H + L \rightleftharpoons H_2L$	15.91(1)	16.02(4)	15.84(4)	16.01(4)	13.40(15)	14.47(5)	17.07(1)	18.69(7)	14.90(1)	15.53(1)
$H + HL \rightleftharpoons H_2L$	7.61(1)	7.65(5)	7.63(5)	7.31(4)	5.91(15)	6.83(5)	8.03(1)	8.53(7)	6.96(1)	7.37(1)

[a] Charges omitted for clarity. [b] Values in parentheses are the standard deviations in the last significant figure. [c] Determined in 0.1 M NaCl using 50 mL of a 2 mM solution of the ligand. [d] Determined in 0.15 M $NaClO_4$ at 298.1 K.[15]

spacers, being very similar for PheA5 and PheA6. Nevertheless, the last two ligands are clearly differentiated by the presence for PheA6 of a hydroxylated [CuH$_{-3}$L] species that is not observed for any other ligand. This suggests the presence of complexes with different molecular structures according to the length of the central spacer. It must be mentioned that the observed trends are significantly different than those found for Val derivatives.[15] Thus, the nature of the side chain also plays a critical role defining the exact species being formed.

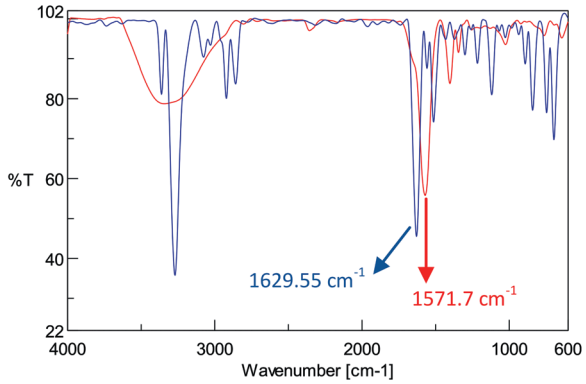

Fig. 3 ATR-FTIR spectra of PheA3 (blue) and CuPheA3 (red) in aqueous solution.

In order to gain a more detailed insight into the nature of the complex species formed by those ligands and Cu^{2+}, a UV-vis spectroscopic study was carried out, taking advantage of the data provided by the distribution diagrams formerly obtained. UV-vis spectra were taken at the most significant regions as defined by the distribution diagrams (Fig. 5). The pH values for the different experiments were adjusted to regions where one major species was defined. The experimental data obtained indicate the existence in solution of several Cu(II) complexes displaying different geometries.[23] In the case of the PheA2 ligand, the spectrum at very high pH values, where [CuH$_{-2}$L] is the only observed species, perfectly agrees with the presence of a square planar complex, with a single band at *ca.* 490 nm. For basic pH values

Table 3 Logarithms of the formation constants for the Cu^{2+} complexes of ligands determined in 0.1 M NaCl at 298.1 ± 0.1 K

Reaction[ac]	PheA2	PheA3	PheA4	PheA5	PheA6
Cu + L ⇌ CuL	—	—	6.35(1)	6.31(3)	6.51(2)
Cu + L + H ⇌ CuHL	—	—	11.35(5)	—	—
Cu + L ⇌ CuH$_{-1}$L + H	1.11(1)[b]	1.12(10)	−0.17(2)	−0.12(3)	−0.39(2)
Cu + L ⇌ CuH$_{-2}$L + 2H	−6.27(1)	−3.88(3)	−6.40(1)	−9.40(5)	−10.24(3)
Cu + L ⇌ CuH$_{-3}$L + 3H	—	—	—	—	−20.95(3)
CuL + H ⇌ CuHL	—	—	5.00(5)	—	—
CuL ⇌ CuH$_{-1}$L + H	—	—	−6.52(2)	−6.43(3)	−6.9(2)
CuH$_{-1}$L ⇌ CuH$_{-2}$L + H	−7.07(1)	−5.00(10)	−6.23(2)	−9.28(5)	−9.85(3)
CuH$_{-2}$L ⇌ CuH$_{-3}$L + H	—	—	—	—	−10.71(3)

[a] Charges omitted for clarity. [b] All values in parentheses are the standard deviations in the last significant figure. [c] Determined in 0.1 M NaCl using 50 mL of a 2 mM solution of the ligand and 1 equiv. of the copper(II) salt.

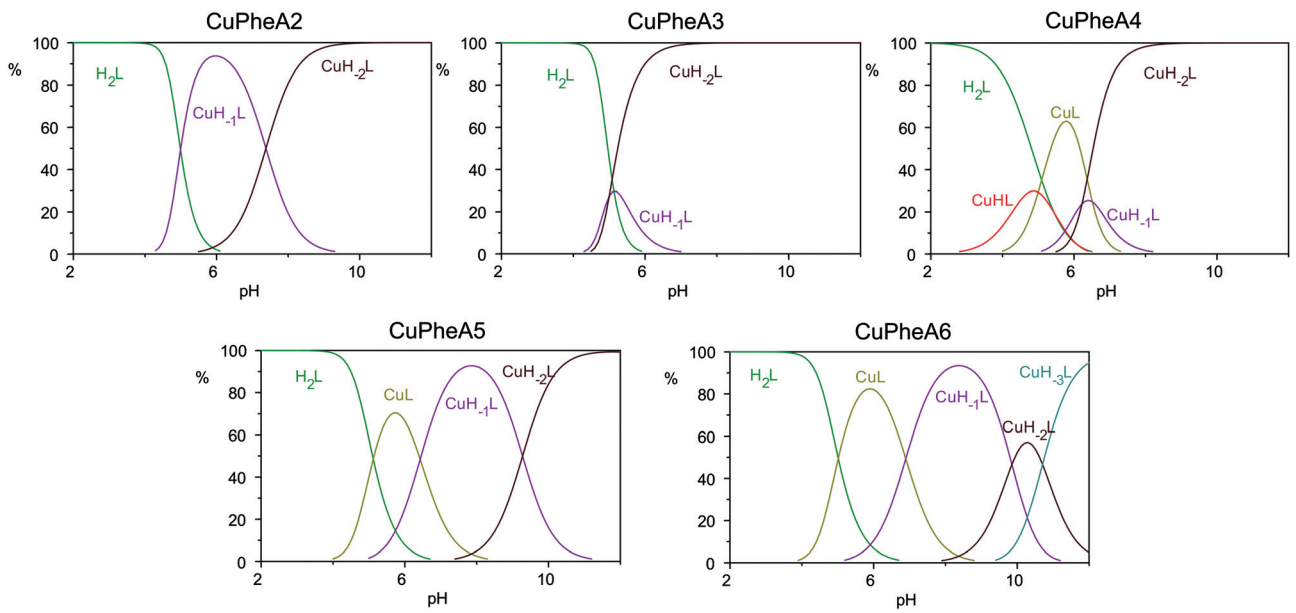

Fig. 4 Species distribution diagrams for the different Cu(II) complexes for PheA2, PheA3, PheA4, PheA5 and PheA6.

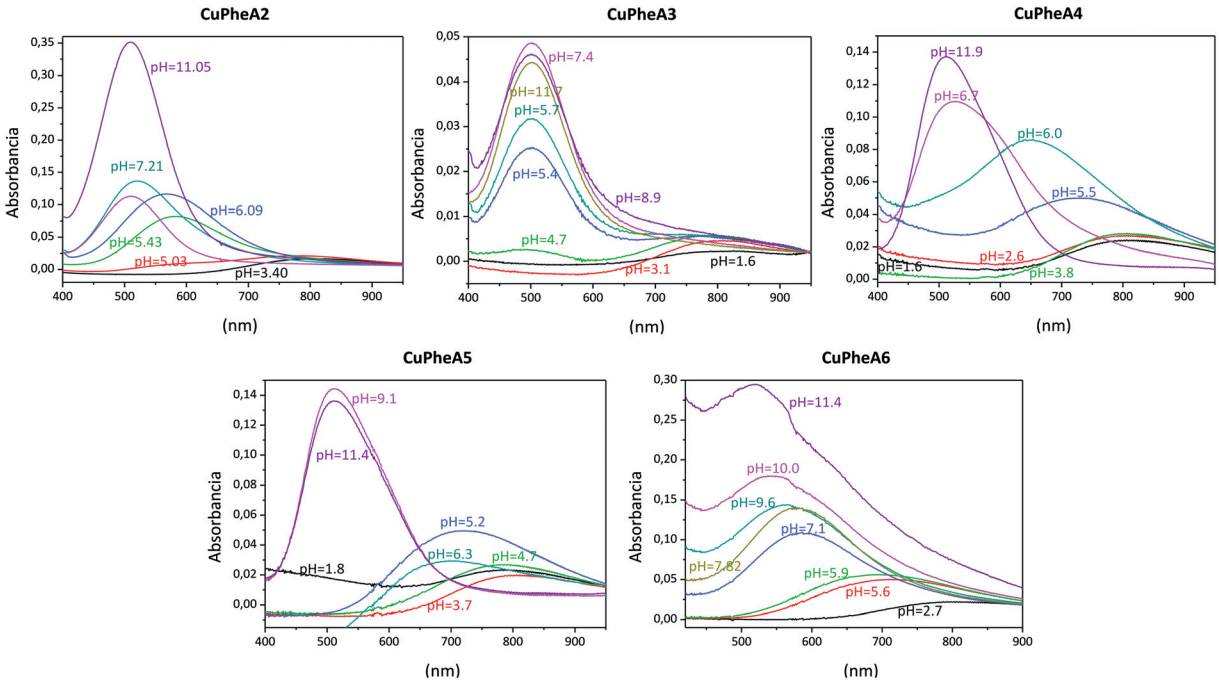

Fig. 5 UV-vis absorption spectra in water for the different Cu(II) complexes for PheA2, PheA3, PheA4, PheA5 and PheA6 at different pH values.

closer to neutrality, where the $[CuH_{-1}L]^{+}$ species is also present (pH 7–8), the former band is transformed with an increase in the absorption at the longer wavelength region, in agreement with the coexistence of a square planar and a square pyramidal complex. At pH = 6, where the $[CuH_{-1}L]^{+}$ species is predominant, a clear band centred at *ca.* 580 nm, which could be ascribed to a square pyramidal complex, is observed. In the acidic region, decomplexation takes place and the band corresponding to Cu^{2+} in an octahedral environment (around 750 nm) is visible. For PheA3, the pure square planar complex survives even at pH values around neutrality, according to the prevalence of the $[CuH_{-2}L]$ species observed in the distribution diagram; as $[CuH_{-1}L]^{+}$ is a minor species, only a small deformation of the square planar band is observed at pH values below 6 and at pH = 4.7 the band centered at *ca.* 500 nm starts to coexist with that of the octahedral non-complexed species. The situation is more complex for ligands with longer spacers, reflecting the presence of additional species in the distribution diagram. For PheA4 and PheA5, even at high pH values square planar and square pyramidal complexes seem to coexist. At pH = 6, where $[CuL]^{2+}$ reaches its maximum concentration but other species are also present, a band centred at 650 nm is observed suggesting the coexistence of square pyramidal and octahedral complexes. Upon acidification, this band is hyprochromically shifted up to obtain again the band corresponding to the octahedral non-complexed Cu^{2+} species. The most complex situation is observed for the PheA6 ligand. A very broad band is observed in the basic region, with its maximum at 520–580 nm. This suggests the coexistence of different complexes with a predominance of the square pyramidal geometry. The observation at very high pH values of a hydroxylated $[CuH_{-3}L]^{-1}$ species must be taken into consideration in this regard. In the region where $[CuH_{-1}L]^{+}$ is very dominant the spectra show the characteristic band for a square pyramidal complex (550–580 nm). For the regions where $[CuL]^{2+}$ is the most important complex, the spectra suggest an octahedral geometry, with a band centred at 700–720 nm. It is interesting to note that the geometries suggested by the UV-vis spectra for $[CuH_{-2}L]$ and $[CuH_{-1}L]^{+}$ species are in agreement with those found in crystallographic structures for Val in ref. 15 and in this work for Phgly and Ala derivatives.

We next investigated the effect of the amino acid side chain on the copper coordination of this kind of ligand. For this purpose, we studied the complexation of ligands with short (n = 0) and long aliphatic spacers (n = 4). The data for the ValA2 and ValA6 ligands had been published previously[15] and they have been included for comparative purposes. The results obtained are presented in Table 4 and in the distribution diagrams in the ESI† and reveal the presence of important differences related to the nature of the side chain.

In general, the complex species with the largest number of methylenes between the amide groups are more stable than the complexes with short aliphatic spacers. As in the case of the acid–base properties, Pro derivatives show a very different behaviour, displaying formation constants for the different complexes that can be one or two orders of magnitude higher than those for the other ligands considered. A detailed analysis of the results obtained allows some trends to be observed. When considering the $[CuL]^{2+}$ species, the stability constants decrease with the size of the side group (Pro is always an exception). Deprotonated species are more stable for the compounds with smaller side chains at the amino acid subunit, in particular for the compounds with the shorter spacer. The general order of stability found, according to the nature of amino acid, can be defined as Phgly ≈ Phe < Val < Ala < Gly < Pro. This may be related to several parameters such as the basicity of the amino

Table 4 Logarithms of the formation constants for the Cu^{2+} complexes of ligands determined in 0.1 M NaCl at 298.1 ± 0.1 K

Reaction[ac]	AlaA2	AlaA6	GlyA2[e]	GlyA6	PhglyA2	PhglyA6	ProA2	ProA6	ValA2[d]	ValA6[d]
Cu + L ⇌ CuL	7.07(3)[b]	7.91(2)	6.72(37)	8.36(2)	—	6.57(1)	8.37(2)	10.29(2)	6.09(4)	7.14(2)
Cu + L + H ⇌ CuHL	12.32(14)	13.52(3)	—	13.76(5)	10.28(6)	11.75(4)	13.87(6)	16.02(4)	—	12.67(6)
Cu + L ⇌ $CuH_{-1}L$ + H	1.44(1)	0.41(2)	0.29(19)	0.54(4)	0.21(1)	−0.42(2)	2.62(2)	3.03(2)	0.67(1)	−0.04(2)
Cu + L ⇌ $CuH_{-2}L$ + 2H	−6.05(2)	−9.84(2)	—	−9.98(4)	−6.66(2)	−10.15(2)	−4.00(1)	−7.12(3)	−6.48(1)	−9.78(3)
Cu + L ⇌ $CuH_{-3}L$ + 3H	—	—	—	—	−13.73(1)	—	—	−19.42(15)	—	—
CuL + H ⇌ CuHL	5.25(14)	5.61(3)	—	5.4(5)	—	5.18(4)	5.50(6)	5.73(4)	—	5.53(5)
CuL ⇌ $CuH_{-1}L$ + H	−5.63(3)	−7.5(2)	−6.43(37)	−7.82(5)	—	−6.99(2)	−5.75(2))	−7.26(2)	−5.42(4)	−7.19(2)
$CuH_{-1}L$ ⇌ $CuH_{-2}L$ + H	−7.49(2)	−10.25(2)	—	−10.52(4)	−6.87(2)	−9.73(2)	−6.62(2)	−10.15(3)	−7.15(1)	−9.74(3)
$CuH_{-2}L$ ⇌ $CuH_{-3}L$ + H	—	—	—	—	−7.07(2)	—	—	−12.3(15)	—	—

[a] Charges omitted for clarity. [b] All values in parentheses are the standard deviations in the last significant figure. [c] Determined in 0.1 M NaCl using 50 mL of a 2 mM solution of the ligand and 1 equiv. of the copper(II) salt. [d] Determined in 0.15 M $NaClO_4$ at 298.1 K.[15] [e] Values for GlyA2 must be considered with caution. Solubility problems lead to less accurate titration curves.

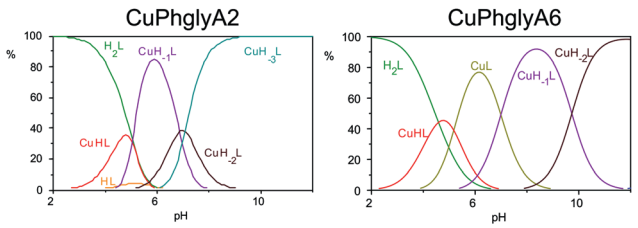

Fig. 6 Distribution diagram for the species of Cu(II) and PhglyA2 and PhglyA6 in 0.1 M NaCl at 298.1 K.

groups and the steric requirements imposed by the different side chains. The analysis of the corresponding distribution diagrams is also illustrative. As an example, the species distribution curves corresponding to the formation of Cu(II) complexes in solutions containing Cu(II) and PhglyA2 and PhglyA6 in 1 : 1 molar ratios are included in Fig. 6. Thus, for the $[CuH_{-2}L]$ species, CuAlaA2 has a similar behaviour to that of CuPheA2. For CuProA2, however, the $[CuH_{-2}L]$ species predominates until slightly more acidic pH values, and $[CuH_{-1}L]^+$ only becomes the major species for a very narrow pH range close to 6. Also, CuGlyA2 behaves differently, with $[CuH_{-1}L]^+$ being predominant for the whole basic region and $[CuL]^{2+}$ around pH 6. For CuPhglyA2 the $[CuH_{-2}L]$ complex species is very minor and the hydroxylated complex $[CuH_{-3}L]^-$ predominates in the basic region. This hydroxylated species is only observed for this ligand.

For the longer spacers, the hydroxylated species $[CuH_{-3}L]^-$ is only observed for CuPheA6. The presence of $[CuHL]^{3+}$ as the major species at pH values around 5 is not observed, however, for CuPhglyA6. In all cases, $[CuH_{-2}L]$ predominates at pH values >10; $[CuH_{-1}L]^+$ is the most important species between pH 10 and around pH 7 and [CuL] is the major species between pH 7 and pH 5. As in the case of the acid–base properties, the interaction with Cu(II) of the ligand AlaA3 was also studied and the results have been included in the ESI.† The general trends observed for the Phe and Val derivatives for intermediate spacer lengths are also presented here. As could be expected, the stability constants for copper(II) complexes of ligands **1** and **2** are significantly lower than those for classical tetranitrogenated ligands, *i.e.* tetraazamacrocycles like cyclam or cyclen.[24] On the other hand, the constants calculated for GlyA2 complexes differ from those previously reported, although being of the same order for [CuL].[20] It must be taken into consideration that methodologies for those calculations are different.

UV-vis spectra (see ESI†) show, as for Phe derivatives, how the absorption maximum shifts from >800 nm to *ca.* 500 nm with increasing pH and the presence of less well defined curves for the longer spacers, in particular at very basic pH values. Only for Pro and Gly derivatives this feature is less pronounced.

ESI-MS is a very useful technique since it allows the detection of species at very low concentrations.[25] As in the case of crystallographic studies, the results need to be handled with care, as the nature of the species in solution could differ from the observations in ESI-MS. In this regard we carried out ESI-MS analyses of the solutions of the different complexes at several pH values of interest as defined by the corresponding distribution diagrams. The ESI technique in the positive mode of analysis was used. Similar results were obtained either in methanol or in water.

An illustrative example is given in Fig. 7 for the complexation of Cu^{2+} by the ligand PheA2 at a pH of around 11. The bisdeprotonated complex species was the base peak ($[(CuH_{-2}PheA2) + Na]^+$ at 438 *m*/*z* and $[(CuH_{-2}PheA2) + K]^+$ at 454 *m*/*z*, *ca.* 100% and 44%). On other hand, there are two peaks for dimeric and trimeric bisdeprotonated copper(II) complexes ($[(CuH_{-2}PheA2)_2 + Na]^+$ at 855 *m*/*z* and $[(CuH_{-2}PheA2)_3 + Na]^+$ at 1271 *m*/*z*). In every case, we have also calculated the simulated peak to check the proper assignation of the signals. Other signals correspond to the mixtures monomer–dimer at 647 *m*/*z* and dimer–trimer bideprotonated copper(II) complexes at 1063 *m*/*z*. At pH 5.4 the main peak was at *m*/*z* 416, assigned to $[CuH_{-1}PheA2]^+$, and some dimeric species involving the monodeprotonated species are also detected. Essentially the same MS is obtained at pH 6.1. At pH values below 5.0, however, the only significant peaks observed correspond to the protonated ligand. Thus, an excellent agreement is observed between the data from ESI-MS and those from potentiometric analysis (Fig. 8). The behaviour of bis(amino amides) with medium-sized aliphatic chains is different due to the emergence of new complex species, according to the distribution diagrams. The MS of the CuPheA4 complexes under strongly basic conditions only shows a peak corresponding to the bisdeprotonated species. Because of its

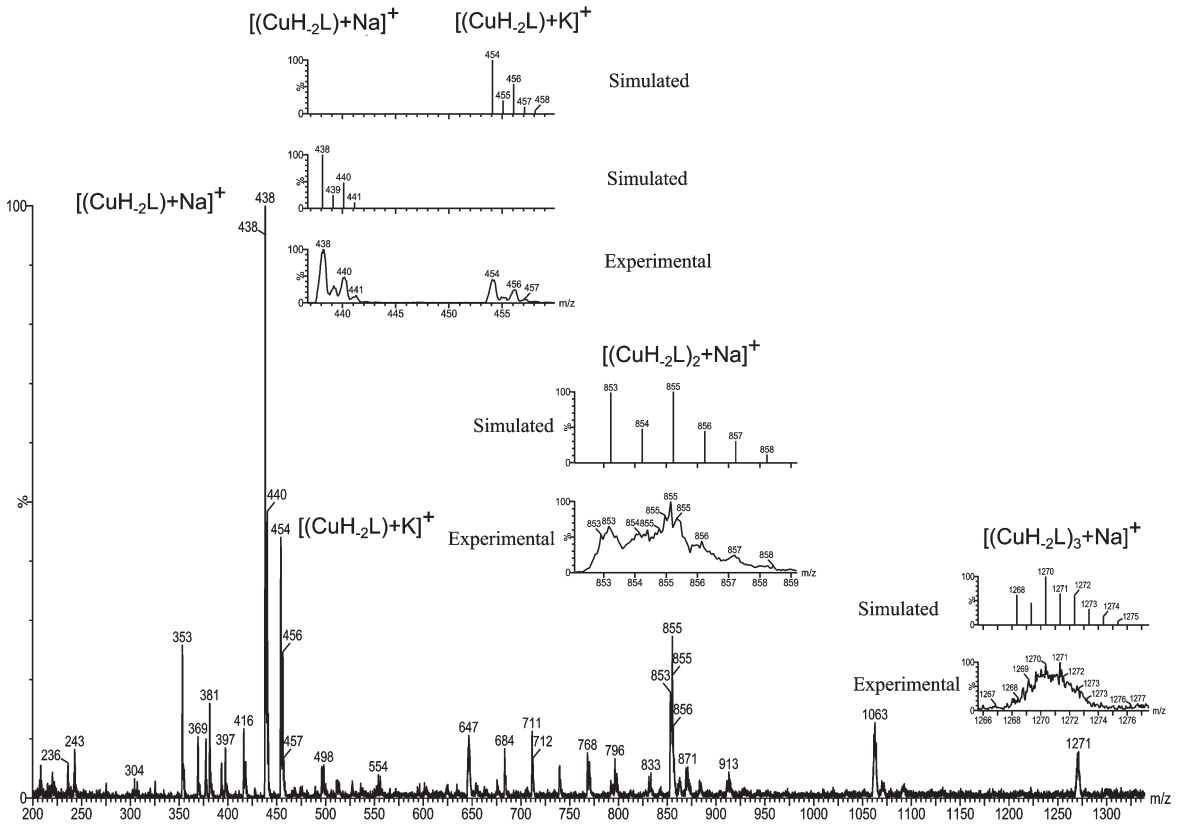

Fig. 7 ESI+ MS spectra for Cu^{2+} complexes with PheA2 at pH = 11 in methanol.

anionic character, the hydroxylated complex could not be detected under our experimental conditions. In this case, even at the neutral region, the peaks corresponding to complex species such as $[CuH_{-1}L]^+$ are very small, and disappear in the acidic region.

On the other hand, the spectra obtained for CuPheA6 at different pH values always show the presence of peaks that can be assigned to the protonated ligand. Only at pH 3.5 is a small peak that can be assigned to the presence of [(CuL) + Cl]− detected. This seems to suggest the predominance of clusters or polymeric complex species for this ligand.

Similar observations are obtained for the complexes of other ligands, with the variations observed in their respective distribution diagrams. Thus, for Cu–GlyA2, the $[CuH_{-1}L]^+$ is predominant at basic pH values and this is also observed by ESI-MS; below pH 5, the only complex species detected is $[CuL]^{2+}$ along with peaks corresponding to the protonated ligand. In general, the ligands with shorter spacers provide ESI-MS spectra at different pH values that can be easily associated to the corresponding distribution diagrams. Only in the case of CuAlaA2, no peaks for complex species can be detected in the basic region. This can be associated to the formation of oligomeric–polymeric complexes with the $[CuH_{-2}L]$ stoichiometry. In agreement with this, the only peak detected for a complex with this stoichiometry is observed at pH = 6.71, corresponding to a dimeric species $[(CuH_{-2}L)_2 + K]^+$. In the case of CuProA2, the presence of dimeric species for this stoichiometry is also important.

On the contrary, in general, for the ligands with the larger spacers, the peaks corresponding to complex species are very minor or completely absent in the MS spectra except for $[CuL]^{2+}$ species, suggesting again the prevalence of polymeric complex species, in particular at very basic pH values. Only for CuGlyA6 and CuAlaA6, significant peaks corresponding to $[CuH_{-1}L]^+$ species are observed.

Crystals suitable for single-crystal X-ray diffraction analysis could be obtained in the case of PhglyA2. A 1 : 1 Cu : PhglyA2 mixture was prepared from $CuCl_2{\cdot}H_2O$ and PhglyA2 in methanol and taken to strongly basic pH using solid KOH (pH = 11). Through a process of slow diffusion with diethyl ether vapor, it was possible to obtain red crystals of good quality. The structure determined for this representative copper(II) complex $[CuH_{-2}(PhglyA2)]$ is shown in Fig. 9 and 10, whereas the most important crystallographic and structural details are gathered in Tables 5 and 6. As is often found, the crystal studies for complexes do not strictly reflect the solution composition observed by potentiometric titrations in water, where a hydroxylated complex species predominates at this pH. The different equilibria can be shifted through the crystallization of a very minor species, in particular taking into account the method of crystallization.

The bond angles formed by the five-membered chelate rings are smaller than 85° and indicate a tight chelation to the copper(II) ion. The N_{amine}–Cu–N_{amine} bite angle at 105.8° is quite spread out and at least 20° larger than the other N–Cu–N angles. The copper(II) ion is 0.072 Å displaced from the N4

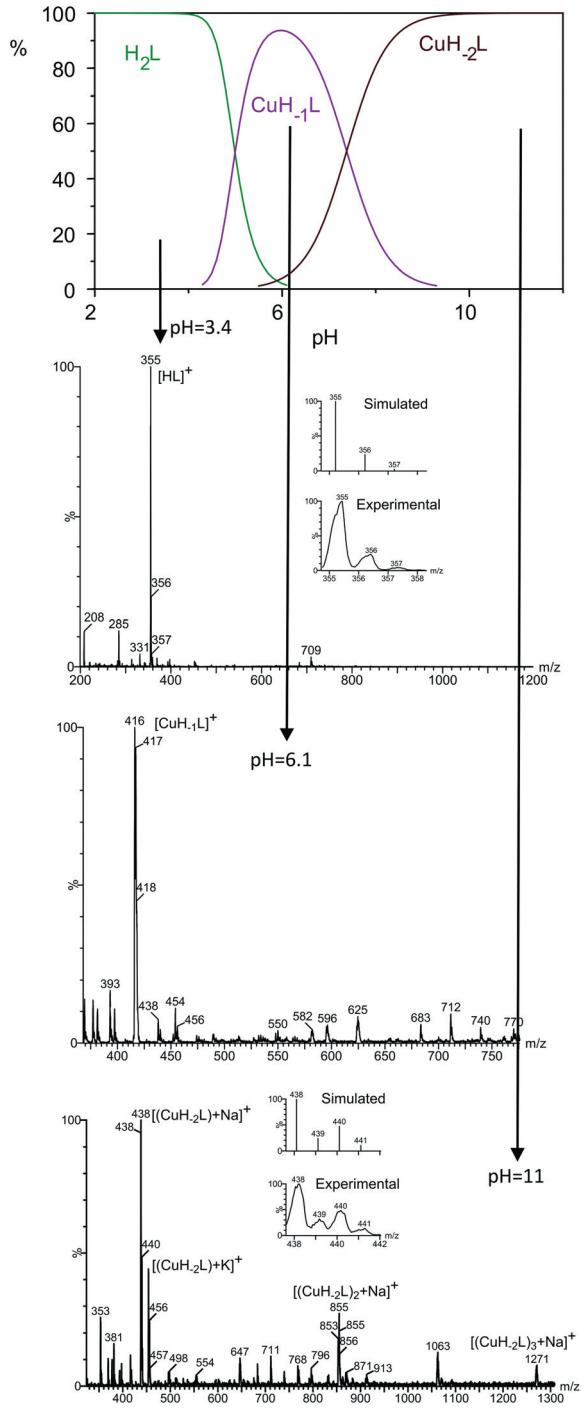

Fig. 8 Matching mass spectra with the species distribution diagram for copper(II) and the ligand PheA2.

basal plane (defined by N1, N2, N3 and N4). The two lateral five-membered chelate planes define an angle of *ca.* 15° with each other, and an angle of 6–11° with the central five-membered chelate ring involving the two Namide groups. The C1 and C7 carbon atoms (see Fig. 9 for the numbering used for the X-ray structure) are significantly out of their respective chelate planes as seen by the N4–C1–C5–N3 and N2–C7–C2–N1 dihedral angles, respectively (Tables 5 and 6). The crystal structure revealed the formation of a mononuclear neutral complex with a

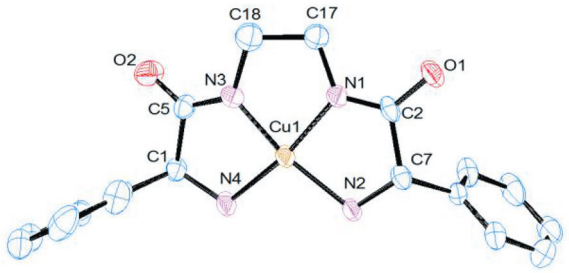

Fig. 9 Molecular structure for the Cu–PhGlyA2 complex obtained at the basic pH region. Thermal ellipsoids are drawn at 30% probability level. Hydrogen atoms are omitted for clarity.

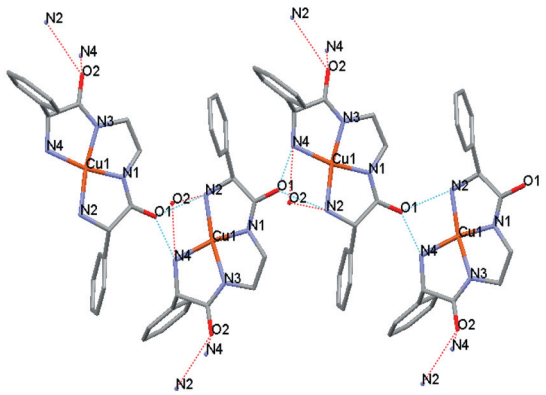

Fig. 10 Schematic representation of the hydrogen bond network for the complex Cu–PhGlyA2 obtained at the basic pH region.

1 : 1 metal : ligand stoichiometry. The copper(II) cation is coordinated by two amine groups and two deprotonated amide groups, in a square planar geometry, as predicted by UV-vis spectroscopy for [$CuH_{-2}L$] species. For this complex, the average Cu–N_{amide} distance of 1.842(2) Å is 0.144 Å shorter than the average Cu–N_{amine} distance of 1.986(2) Å. This difference may be attributed to the anionic coordination from the deprotonated N_{amide} donors instead of the neutral donation from the N_{amine} groups.

Bifurcated hydrogen bonds are formed between the carbonyl oxygen atom O1 of one of the molecules and an hydrogen of the amine nitrogen atoms N2 and N4 of a second molecule (O1–N2 2.93 Å, O1–N4 2.91 Å). The other carbonyl oxygen atom of the first molecule (O2) is also hydrogen bonded, in the same way, to a third molecule (O2–N2 2.86 Å, O2–N4 3.04 Å). Fig. 10 depicts the hydrogen bond network formed.

Suitable crystals of Cu–PheA3 were grown by slow evaporation of a solution of $CuCl_2 \cdot H_2O$ and PheA3 in methanol, in the absence of any base. As can be seen in the distribution diagrams for Cu–PheA3, the [$CuH_{-2}L$] species predominate up to pH values above 6. So, in this case, the obtained crystallographic structure corresponds to the predominant complex predicted at that pH value from the distribution diagram. The copper(II) ion is again coordinated by two deprotonated N_{amide} atoms and two neutral N_{amine} centres in a square-planar geometry with an average Cu–N_{amide} distance of 1.930(9) Å and Cu–N_{amine} distance of 2.011(5) Å (see Fig. 11). As in the other case, the N–Cu distances are similar to the ones observed in other Cu(II) complexes with related ligands.[26] In general, structural parameters

Table 5 Selected bond lengths [Å] and angles [°] for Cu–PhglyA2 and Cu–PheA3 crystal structures

Distance or angle	CuPhglyA2	CuPheA3
Cu–N1	1.895(4)	2.006(7)
Cu–N2	1.987(4)	1.940(8)
Cu–N3	1.877(5)	1.919(7)
Cu–N4	1.990(4)	2.016(8)
N2–Cu–N3	169.55(18)	96.6(3)
N3–Cu–N4	84.68(19)	173.3(3)
N2–Cu–N4	105.76(18)	98.4(3)
N1–Cu–N3	84.80(2)	171.8(3)
N1–Cu–N2	84.82(18)	83.0(3)
N1–Cu–N4	167.6(2)	98.4(3)

Table 6 Crystallographic data for Cu–PhGlyA2 and Cu–PheA3 crystal structures

	CuPhglyA2	CuPheA3
Empirical formula	C_{18} H_{20} Cu N_4 O_2	C_{23} H_{34} Cu N_4 O_4
Formula mass	387.92	494.08
T [K]	298	298
Crystal system	Orthorhombic	Orthorhombic
Space group	$P2_12_12_1$	$P2_12_12_1$
Color	Red	
Crystal size mm	0.28 × 0.28 × 0.18	0.46 × 0.31 × 0.22
a [Å]	10.4048(11)	9.5315(2)
b [Å]	11.3542(13)	12.0135(3)
c [Å]	14.9983(18)	20.7584(4)
α [°]	90	90
β [°]	90	90
γ [°]	90	90
V [Å^3]	1771.9(3)	2376.98(9)
Z	4	4
D_{calcd} [g cm^{-3}]	1.454	1.381
Absorption coefficient [mm^{-1}]	1.251	0.955
R^a	0.0500	0.0257
Rw^b	0.1040	0.0648
GOF on F^2	1.017	1.012

^{a} $R = \sum||F_o| - |F_c||/\sum|F_o|$ ^{b} $R_w = \{[\sum(|F_o|^2|F_c|^2)^2]\}^{1/2}$.

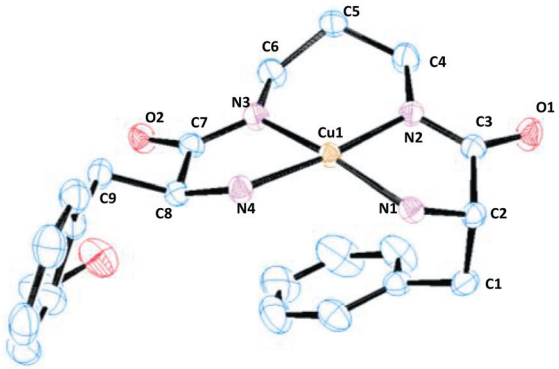

Fig. 11 Molecular structure obtained for the complex Cu–PheA3 in the absence of added base, pH = 6. Thermal ellipsoids are drawn at 30% probability level. Hydrogen atoms are omitted for clarity.

Table 7 Interatomic distances in the amide N–C–O moiety and for the amino group

	C=O	C–N_{amina}	C–N_{amida}
PheA2	1.239	1.469	1.337
CuPheA3	1.271	1.474	1.310
CuPhglyA2	1.251	1.497	1.312
Cu-macrocycle[26]	1.262	1.473	1.305

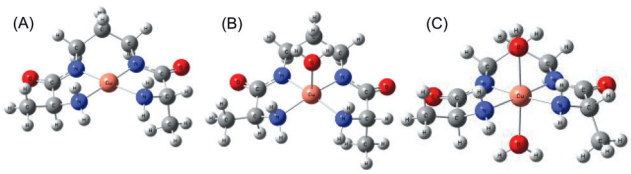

Fig. 12 Optimized geometries for the square planar complex (A), the square pyramidal complex (B) and the octahedral complex (C) used as a model starting from the deprotonated AlaA3 ligand.

for this structure are very much like those found for the Cu–PhglyA2 system under basic conditions, although angles and distances are slightly higher for the Phe derivative (Table 7).

As mentioned above, the angles and interatomic distances observed in both crystalline structures are in good agreement with those found in related systems. As an example, Table 7 shows some selected interatomic distances for the two crystal structures and their comparison with those in a free ligand and in the Cu(II) complex of a macrocyclic bis(amino amide) ligand recently described.[26]

DFT studies were carried out to obtain some additional information about the nature of the species formed. The calculations were done by optimizing the geometries both in the gas phase and in solution (CPCM model) to obtain a better approximation to the experimental conditions. However, the geometries derived must be taken with care not only because of the limitations implicit in the calculations but also because additional factors as hydrogen bonding with solvent molecules were not included in the model. A simple Ala derivative (AlaA3) was selected for this study in order to reduce the number of atoms involved. The structures of the square planar, square pyramidal and octahedral complexes (with water as the additional ligand) for the deprotonaded bis(amino amide) were optimized and are presented in Fig. 12.

Once the optimized geometries were obtained, the corresponding calculated spectra were obtained using the CPCM/TD-DFT approach, and the values for the λ (nm) of the most intense transition of each one are presented in Table 8. Thus, DFT calculations provide a reasonable explanation to the experimental observation of the UV-vis spectra. From the results presented in Table 8, it seems reasonable to assume that the experimental absorption band centered at 500 nm can correspond to a mixture of two different geometries involving a square planar tetradentate complex and a square pyramidal complex, in which the fifth coordination site is occupied by a water molecule. The energy values in Table 8 show that the square pyramidal complex is slightly lower in energy than the square planar one and, thus, the potential coexistence of these two species with different geometries, in an aqueous environment, is reasonable. The results shown in the ESI† for AlaA3 are also in good agreement with this analysis.

Conclusions

In this work, we have shown that bis(amino amide) ligands are able to form complexes of very different structures with Cu^{2+}. A combination of different techniques such as, pH-metric titrations, spectroscopic studies, ESI MS experiments and DFT calculations has been carried out to analyze the complex formation. The critical factors determining the final structure of the complexes are the nature of the aliphatic spacer connecting the two amino acid subunits and the pH value at which the complex is formed, and also the amino acid side chain residue. Important variations in the nature of the predominant complex species formed at each pH value can be observed when the corresponding distribution diagrams are analyzed. It is worth mentioning how the Pro derivatives provide a very particular situation, both in terms of their basicity and in terms of the nature of the complexes formed. In general, ligands containing aliphatic side chains display higher basicities as well as stability constants with Cu^{2+}. In the same way, basicities and stability constants tend to increase when decreasing the steric hindrance caused by the corresponding side-chain. UV-vis spectroscopy and DFT studies suggest the existence of different geometries in this kind of copper(II) complex. In particular, for the complexes formed by bis deprotonated ligands containing shorter spacers, the square planar complex and square pyramidal seem to coexist. The crystal structures determined for two such copper(II) complexes derived from PhglyA2 and PheA3 confirm the results obtained with the other techniques, with the observation of well defined square planar coordination spheres in the crystal structure. Finally, as was observed in the case of Val derivatives, ESI-MS experiments are in good agreement with the calculated distribution diagrams, which indicate that, most likely, clusters or polymeric structures are formed for the complexes of the ligands containing the larger central spacers.

Experimental section

Materials and reagents

All reagents were obtained from commercial sources and used as received unless otherwise stated. Dimethoxyethane (DME) was dried and distilled from molecular sieves (4 Å) and then stored over molecular sieves. Diethyl ether was dried by refluxing in the presence of sodium wire under an inert gas. Deionised water was used from a Milli-Q water system by Millipore.

General procedure for the synthesis of Cbz-*N*-protected bis(amino amide) ligands

The *N*-hydroxysuccinimide ester (1 mmol) was dissolved in anhydrous DME (30 mL) and cooled in an ice bath. A solution of diamine (0.5 mmol) in anhydrous DME was added dropwise. The reaction mixture was stirred at room temperature for 2 h, then refluxed for 5 h and maintained for 8 h at 40–50 °C. The white solid was filtered and washed with alkaline and neutral water. The obtained compound showed high purity by NMR and was used in the next step without further purification steps.

General procedure for the deprotection of Cbz-*N*-protected bis(amino amide) ligands

A HBr–AcOH 33% solution (20 mL) was slowly added to the Cbz-*N*-protected bis(amino amide) ligand and the mixture was stirred at room temperature until CO_2 evolution ceased. At this point, diethyl ether was added to the clear solution, which led to the deposition of a white precipitate. This was filtered off, washed with additional ether and dissolved in distilled water; the resulting solution was extracted with chloroform (3 × 15 mL). Solid NaOH was added up to a pH value of 12 and the resulting solution was saturated with NaCl and extracted with chloroform (3 × 15 mL). The organic phase was dried over Mg_2SO_4 and evaporated under vacuum to obtain a white solid.

The following compounds were prepared by known methods: *N*,*N*′-bis(*N*-Cbz-L-phenylalanine)-1,2-diaminoetane (PheA2),[6b] *N*,*N*′-bis(*N*-Cbz-L-phenylalanine)-1,3-diaminopropane (PheA3),[6b] *N*,*N*′-bis(*N*-Cbz-L-phenylalanine)-1,4-diaminobutane (PheA4),[6b] *N*,*N*′-bis(*N*-Cbz-L-phenylalanine)-1,5-diaminopentane (PheA5),[6b] *N*,*N*′-bis(*N*-Cbz-L-phenylalanine)-1,6-diaminohexane (PheA6),[6b] *N*,*N*′-bis(*N*-Cbz-L-glycine)-1,2-diaminoetane (GlyA2),[9c] *N*,*N*′-bis(*N*-Cbz-L-Alanine)-1,2-diaminoetane (AlaA2),[9c] and *N*,*N*′-bis(*N*-Cbz-L-Alanine)-1,3-diaminopropane (AlaA3).[9c]

Synthesis of *N*,*N*′-bis(*N*-Cbz-L-Phenyglycine)-1,2-diaminoetane, PhglyA2

This compound was obtained as described above starting from *N*,*N*′-bis(*N*-Cbz-L-phenyglycine)-1,2-diaminoetane and HBr–AcOH solution. Yield = 20%; m.p. = 90.7 °C; $[\alpha]_D^{25}$ = 39.6° (*c* = 0.1, $CHCl_3$); ESI-MS *m*/*z* = 327.1 ($M + H^+$); IR ν_{max} = 3481, 3297, 2917, 2849, 1647, 1517, 1305 cm^{-1}; ^1H NMR (500 MHz, $CDCl_3$, 25 °C) δ = 1.75 (s, 4H), 3.38 (d, 4H, *J* = 22.3 Hz), 4.39 (s, 2H), 7.34 (s, 10H), 7.43 (s, 2H); ^{13}C NMR (125 MHz,

Table 8 Summary of the relative energies[a] and λ_{max} (nm) values calculated for the different gas-phase and solution optimized geometries for the Cu^{2+} complexes with AlaA3

	Relative energy (kcal mol^{-1})			λ_{max}[b] (nm)		
Species	Gas	Water	Methanol	Gas	Water	Methanol
A	0.0	0.0	0.0	396.47	425.89	426.64
B	−0.1	−1.2	−1.5	568.76	559.57	560.84
C	+12.8	+35.0	+33.5	743.78	759.33	765.21

[a] The relative gas energy values correspond to CPCM single-point calculations on the previously gas-phase optimized structures. [b] These values correspond to the λ (nm) of the most intense transition of each calculated spectra using the CPCM/TD-DFT approach.

$CDCl_3$, 25 °C) δ = 38.8, 59.6, 127.1, 127.3, 127.5, 128.4, 128.6, 143.1, 174.0; Elemental analysis calcd (%) for $C_{18}H_{22}N_4O_2$: C, 66.24; H, 6.79; N, 17.17. Found: C, 66.685; H, 7.137; N, 16.804.

Synthesis of *N*,*N*′-bis(*N*-Cbz-L-Phenyglycine)-1,6-diaminohexane, PhglyA6

This compound was obtained as described above starting from *N*,*N*′-bis(*N*-Cbz-L-phenyglycine)-1,6-diaminohexane and HBr–AcOH solution. Yield = 78%; m.p. = 106 °C; $[\alpha]_D^{25}$ = 37.26° (*c* = 0.1, $CHCl_3$); ESI-MS *m*/*z* = 383.24 (M + H^+); IR ν_{max} = 3375, 3306, 2923, 2852, 1634, 1539, 1310 cm^{-1}; ^1H NMR (500 MHz, $CDCl_3$, 25 °C) δ = 0.37 (d, 4H, *J* = 10.6 Hz), 0.54 (d, 4H, *J* = 6.4 Hz), 1.69 (d, 4H, *J* = 1.1 Hz), 2.12–2.30 (m, 4H), 3.62 (s, 2H), 6.14–6.40 (m, 3H), 6.40–6.47 (m, 3H), 6.54 (d, 4H, *J* = 7.7 Hz), 6.90–7.00 (m, 2H); ^{13}C NMR (125 MHz, $CDCl_3$, 25 °C) δ = 25.9, 29.3, 38.7, 59.9, 126.8, 127.9, 128.8, 141.2, 172.9; Elemental analysis calcd (%) for $C_{22}H_{30}N_4O_2$: C, 69.08; H, 7.91; N, 14.65. Found: C, 69.678; H, 7.027; N, 13.526.

Synthesis of *N*,*N*′-bis(*N*-Cbz-L-Proline)-1,2-diaminoetane, ProA2

This compound was obtained as described above starting from *N*,*N*′-bis(*N*-Cbz-L-proline)-1,2-diaminoetane and HBr–AcOH solution.Yield = 76%; m.p. = 113.1 °C; $[\alpha]_D^{25}$ = −86.7° (*c* = 0.1, $CHCl_3$); ESI-MS *m*/*z* = 255.17 (M + H^+); IR ν_{max} = 3277, 3085, 2950, 2853, 1641, 1548, 1241 cm^{-1}; ^1H NMR (500 MHz, $CDCl_3$, 25 °C) δ = 1.21 (s, 2H), 1.57–1.75 (m, 4H), 1.79–1.88 (m, 2H), 2.02–2.15 (m, 2H), 2.81–2.91 (m, 2H), 2.93–3.01 (m, 2H), 3.26–3.40 (m, 4H), 3.69 (dd, 2H, *J* = 5.4, 9.0 Hz), 7.88 (s, 2H); ^{13}C NMR (125 MHz, $CDCl_3$, 25 °C) δ = 26.0, 30.7, 39.0, 47.1, 60.5, 175.7; Elemental analysis calcd (%) for $C_{12}H_{22}N_4O_2$: C, 56.07; H, 8.72; N, 22.03 Found: C, 57.946; H, 8.033; N, 20.524.

Synthesis of *N*,*N*′-bis(*N*-Cbz-L-Proline)-1,6-diaminohexane, ProA6

This compound was obtained as described above starting from *N*,*N*′-bis(*N*-Cbz-L-proline)-1,6-diaminohexane and HBr–AcOH solution. Yield = 64%; m.p. = 53 °C; $[\alpha]_D^{25}$ = −2.14° (*c* = 0.1, $CHCl_3$); ESI-MS *m*/*z* = 297.22 (M + H^+); IR ν_{max} = 3286, 2928, 2859, 1630, 1526 cm^{-1}; ^1H NMR (500 MHz, $CDCl_3$, 25 °C) δ = 1.30 (d, 4H, *J* = 1.9 Hz), 1.42–1.50 (m, 4H), 1.60–1.72 (m, 4H), 1.85 (dd, 2H, *J* = 6.8, 12.8 Hz), 2.02–2.12 (m, 4H), 2.79–2.90 (m, 2H), 2.91–3.01 (m, 2H), 3.17 (dt, 4H, *J* = 3.8, 7.3 Hz), 3.61–3.71 (m, 2H), 7.58 (s, 2Hs); ^{13}C NMR (125 MHz, $CDCl_3$, 25 °C) δ = 26.1, 26.4, 29.5, 30.7, 38.6, 47.2, 60.6, 175.0. Elemental analysis calcd (%) for $C_{16}H_{30}N_4O_2$: C, 61.90; H, 9.74; N, 18.05 Found: 61.704; H, 8.569; N, 17.278.

Synthesis of *N*,*N*′-bis(*N*-Cbz-L-Alanine)-1,6-diaminohexane, AlaA6

This compound was obtained as described above starting from *N*,*N*′-bis(*N*-Cbz-L-alanine)-1,6-diaminohexane and HBr–AcOH solution. Yield = 78%; m.p. = 53 °C; $[\alpha]_D^{25}$ = −7.0° (*c* = 0.1, $CHCl_3$); ESI-MS *m*/*z* = 259.2 (M + H^+), 281.2 (M + Na^+); IR ν_{max} = 3316, 3285, 2918, 2850, 1635, 1534, 1231 cm^{-1}; ^1H NMR (500 MHz, $CDCl_3$, 25 °C) δ = 1.22–1.24 (d, 6H, *J* = 6.9 Hz), 1.26–1.28 (m, 4H), 1.41–1.45 (m, 4H), 2.83 (s br, 2H), 3.11–3.17 (m, 4H), 3.34–3.41 (d, 2H, *J* = 6.9 Hz); ^{13}C NMR (125 MHz, $CDCl_3$, 25 °C) δ = 17.2, 26.1, 29.1, 38.7, 50.4, 169.9. Elemental analysis calcd (%) for $C_{12}H_{26}N_4O_2$: C, 55.79; H, 10.14; N, 21.69. Found: C, 55.557; H, 8.274; N, 20.936.

Synthesis of *N*,*N*′-bis(*N*-Cbz-L-Glycine)-1,6-diaminohexane, GlyA6

This compound was obtained as described above starting from *N*,*N*′-bis(*N*-Cbz-L-glycine)-1,6-diaminohexane and HBr–AcOH solution. Yield = 10%; m.p. = 111–113 °C; ESI-MS *m*/*z* = 230.17 (M + H^+); IR ν_{max} = 3275, 3228, 1646, 1569, 1536 cm^{-1}; ^1H NMR (500 MHz, DMSO) δ = 1.23 (dd, *J* = 8.5, 5.3 Hz, 2H), 1.41–1.34 (m, 2H), 2.52–2.45 (m, 2H), 3.04 (dd, *J* = 13.0, 6.5 Hz, 4H), 7.72 (s, 1H), ^{13}C NMR (126 MHz, DMSO) δ = 26.54, 29.62, 38.60, 45.20, 173.10; Elemental analysis calcd for (%) $C_{10}H_{22}N_4O_2$: C, 52.15; H, 9.63; N, 24.33. Found: C, 51.587; H, 9.154; N, 22.325.

Electromotive force measurements

The potentiometric titrations were carried out at 298.1 ± 0.1 K using NaCl 0.1 M as supporting electrolyte. The experimental procedure (burette, potentiometer, cell, stirrer, microcomputer, *etc*.) has been fully described elsewhere.[27] The acquisition of the emf data was performed with the computer program CrisonCapture. The reference electrode was an Ag–AgCl electrode in saturated KCl solution. The glass electrode was calibrated as a hydrogen-ion concentration probe by titration of previously standardized amounts of HCl with CO_2-free NaOH solutions and the equiv. point determined by the Grańs method, which gives the standard potential, $E°'$, and the ionic product of water [p*K*w = 13.78(1)]. The computer program HYPERQUAD[28] was used to calculate the protonation and stability constants, and the HySS[29] program was used to obtain the distribution diagrams. The pH range investigated was 2.0–12.0 and the concentration of the metal ions and of the ligands ranged from 1×10^{-3} to 5×10^{-3} M with Cu^{2+} : L molar ratios as 1 : 1. The different titration curves for each system (at least two) were treated either as a single set or as separated curves without significant variations in the values of the stability constants. Finally, the sets of data were merged together and treated simultaneously to give the final stability constants.

NMR measurements

The ^1H spectra were recorded on a Varian INOVA 500 spectrometer (500 and 125 MHz for ^1H and ^{13}C NMR, respectively). The solvent signal was used as a reference standard. Adjustments to the desired pH were made using drops of DCl or NaOD solutions. The pD was calculated from the measured pH values using the correlation, pH = pD − 0.4.[30]

Mass spectrometry

Mass spectra were recorded on a hybrid QTOF I (quadrupole-hexapole-TOF) mass spectrometer with an orthogonal Z-spray-electrospray interface (Micromass, Manchester, UK) either by electrospray positive mode (ES+) or by electrospray negative mode (ES−). The desolvation gas as well as nebulizing gas was nitrogen at a flow of 700 L h^{-1} and 20 L h^{-1}, respectively. The temperature of the source block was set to 120 °C and the desolvation temperature to 150 °C. A capillary voltage of 3.5 and 3.3 kV was used in the positive and negative scan mode, respectively. The cone voltage was typically set to 20 V to control the extent of fragmentation of the identified ions. Sample solutions were infused *via* syringe pump directly connected to the ESI source at a flow rate of 10 mL min^{-1}. The observed isotopic pattern of each intermediate perfectly matched the theoretical isotope pattern calculated from their elemental composition using the MassLynx 4.0 program.

UV-vis spectroscopy

UV-vis absorption spectra were recorded in MeOH, in a Hewlett-Packard 8453 apparatus, using solutions (1×10^{-3} M) at different pH values containing 1 : 1 ligand to metal molar ratios. Additional experiments were carried out in NaCl 0.1 M solutions. Only minimal differences were observed in this case.

IR spectroscopy

FTIR spectra were acquired on a JASCO 6200 equipment with a MIRacle single-reflection ATR diamond/ZnSe accessory. The raw IR spectral data were processed with the JASCO spectral manager software. Solutions (2×10^{-3} M) at different pH values containing 1 : 1 ligand to metal molar ratios were used for those experiments.

DFT calculations

All DFT calculations were carried out with the Gaussian 03 software package using the B3LYP level. All structures were computed using the density functional theory using the non-local hybrid Becke's three-parameter exchange functional (denoted as B3LYP) with effective core LanL2DZ pseudopotential and the associated basis set for Cu(II) and the 6-31G (d) basis set for the rest of ligand atoms (C, N, O, H). All geometry optimizations were performed without any symmetry constraints both in gas phase and in solvent, and efforts were made to find the lowest energy conformations by comparing the structures optimized from different starting geometries. Aqueous-phase calculations (ε 78.39) were performed through the use of the conductor-like polarizable continuum model (CPCM) as implemented in Gaussian 03. In order to take into account the non-specific water effect in the gas-phase geometry optimizations, the energy of the species obtained in the gas phase is given in the text as the result of single-point CPCM calculations. Vibrational calculations were performed to confirm that the calculated structures were true minima. The electronic absorption spectra of the previously optimized species were calculated using the time-dependent DFT (TD-DFT) formalism, and 50 singlet-excited-state energies were calculated, respectively. The non-specific solvent effect was considered in the TD-DFT calculations *via* the non-equilibrium version of the CPCM algorithm.

Crystallography

The crystals are air stable and were mounted on the tip of a glass fiber with the use of epoxi cement. X-Ray diffraction experiments were carried out on a Bruker SMART CCD diffractometer using Mo-Kα radiation (λ = 0.71073 Å) at room temperature. The data were collected with a frame width of 0.3° in ω and a counting time of 40 s per frame at a crystal to detector distance of 4 cm. The diffraction frames were integrated using the SAINT package and corrected for absorption with SADABS.[31] The structures were solved by direct methods and refined by the full-matrix method based on F^2 using the SHELXTL software package.[32] All non-hydrogen atoms were refined anisotropically and hydrogen atoms were generated geometrically, assigned isotropic thermal parameters and allowed to ride on their respective parent carbon atoms.[33] Intermolecular C–H···N and C–H···O contacts were examined with the DIAMOND 2.0 package.[34] Cambridge Crystallographic Data Centre CCDC 801764 (CuPhglyA2) and CCDC 829491 (CuPheA3) contain the supplementary crystallographic data for this paper.†

Acknowledgements

Financial support from Ministerio de Ciencia e Innovación (MCIN, CTQ2009-14366-C02-01) and Bancaja-UJI (P1-1B-2009-59) is gratefully acknowledged. I. M. thanks MCINN for a predoctoral fellowship. A. F. thanks Universitat Jaume I for the financial support under the program "Pla de promoció de la investigació". The authors are grateful to the SCIC of the Universitat Jaume I for the spectroscopic facilities.

Notes and references

1 (*a*) F. Meyer and H. Kozlowski, *Comprehensive Coordination Chemistry II: From Biology to Nanotechnology*, ed. J. A. McCleverty and T. J. Meyer, Elsevier, Oxford, 2004, vol. 6, p. 247; (*b*) G. A. Lawrance, *Introduction to Coordination Chemistry*, John Wiley & Sons Ltd, Chichester, 2010, pp. 233–245.
2 (*a*) A. E. Martell and R. J. Motekaitis, *Coord. Chem. Rev.*, 1990, **100**, 323; (*b*) A. E. Martell and R. D. Hancock, *Metal Complexes in Aqueous Solutions*, Plenum Press, New York, 1995; (*c*) J. Gao, J. H. Reibenspies, R. A. Zingaro, F. R. Woolley, A. E. Martell and A. Clearfield, *Inorg. Chem.*, 2005, **44**, 232.
3 (*a*) J.-M. Lehn, *Angew. Chem., Int. Ed.*, 1988, **27**, 89; (*b*) F. P. Schmidtchen, *Top. Curr. Chem.*, 1986, **132**, 101; (*c*) M. E. Huston, E. U. Akkaya and A. W. Czarnik, *J. Am. Chem. Soc.*, 1989, **111**, 8735; (*d*) B. Dietrich, *Pure Appl. Chem.*, 1993, **65**, 1457–1464; (*e*) J.-M. Lehn, *Supramolecular Chemistry. Concepts and Perspective*, VCH, Weinheim, Germany, 1995; (*f*) A. Bianchi, K. Bowman-James and E. Garcia-España, *Supramolecular Chemistry of Anions*, Wiley-VCH, New York, 1997; (*g*) P. D. Beer, *Acc. Chem. Res.*, 1998, **31**, 71; (*h*) A. Bencini, A. Bianchi, E. García-España, M. Micheloni and J. A. Ramírez, *Coord. Chem. Rev.*, 1999, **188**, 97; (*i*) P. D. Beer and P. A. Gale, *Angew. Chem., Int. Ed.*, 2001, **40**, 486; (*j*) P. A. Gale, *Coord. Chem. Rev.*, 2001, **213**, 79.
4 (*a*) S. K. Burke, Y. Xu and D. W. Margerum, *Inorg. Chem.*, 2003, **42**, 5807; (*b*) B. J. Green, T. M. Tesfai and D. W. Margerum, *Inorg. Chem.*, 2004, **43**, 1463; (*c*) B. J. Green, T. M. Tesfai and D. W. Margerum,

Dalton Trans., 2004, 3508; (*d*) T. M. Tesfai, B. J. Green and D. W. Margerum, *Inorg. Chem.*, 2004, **43**, 6726; (*e*) J.-C. Kizirian, *Chem. Rev.*, 2008, **108**, 140; (*f*) J. S. Prell, T. G. Flick, J. Oomens, G. Berden and E. R. Williams, *J. Phys. Chem. A.*, 2010, **114**, 854; (*g*) S. K. Sharma, G. Hundal and R. Gupta, *Eur. J. Inorg. Chem.*, 2010, 621.

5 M. I. Burguete, M. Collado, J. Escorihuela and S. V. Luis, *Angew. Chem., Int. Ed.*, 2007, **46, 47**, 9005; M. I. Burguete, J. Escorihuela, S. V. Luis, A. Lledós and G. Ujaque, *Tetrahedron*, 2008, **64, 41**, 9724.

6 (*a*) F. Adrián, M. I. Burguete, S. V. Luis, J. F. Miravet, M. Querol and E. García-España, *Tetrahedron Lett.*, 1999, **40**, 1039; (*b*) J. Becerril, M. Bolte, M. I. Burguete, F. Galindo, E. García-España, S. V. Luis and J. F. Miravet, *J. Am. Chem. Soc.*, 2003, **125**, 6677.

7 (*a*) M. Bru, I. Alfonso, M. I. Burguete and S. V. Luis, *Tetrahedron Lett.*, 2005, **46**, 7781; (*b*) I. Alfonso, M. Bolte, M. Bru, M. I. Burguete and S. V. Luis, *Chem.–Eur. J.*, 2008, **14**, 8879.

8 (*a*) M. Bru, I. Alfonso, M. I. Burguete and S. V. Luis, *Angew. Chem., Int. Ed.*, 2006, **45**, 6155; (*b*) I. Alfonso, M. Bolte, M. Bru, M. I. Burguete, S. V. Luis and J. Rubio, *J. Am. Chem. Soc.*, 2008, **130**, 6137.

9 (*a*) B. Escuder, J. F. Miravet, R. Gavara and S. V. Luis, *Eur. J. Org. Chem.*, 2005, 481; (*b*) J. Becerril, M. I. Burguete, B. Escuder, S. V. Luis, J. F. Miravet and M. Querol, *Chem. Commun.*, 2002, 738; (*c*) J. Becerril, M. I. Burguete, B. Escuder, F. Galindo, R. Gavara, J. F. Miravet, S. V. Luis and G. Peris, *Chem.–Eur. J.*, 2004, **10**, 3879; (*d*) M. I. Burguete, F. Galindo, R. Gavara, M. A. Izquierdo, J. C. Lima, S. V. Luis, A. J. Parola and F. Pina, *Langmuir*, 2008, **24**, 9795; (*e*) M. I. Burguete, M. A. Izquierdo, F. Galindo and S. V. Luis, *Chem. Phys. Lett.*, 2008, **460**, 503.

10 F. Galindo, M. I. Burguete, L. Vigara, S. V. Luis, N. Kabir, J. Gavrilovic and D. A. Russell, *Angew. Chem., Int. Ed.*, 2005, **44**, 6504.

11 (*a*) M. I. Burguete, F. Galindo, M. A. Izquierdo, S. V. Luis and L. Vigara, *Tetrahedron*, 2007, **63**, 9493; (*b*) I. Alfonso, M. I. Burguete, F. Galindo, S. V. Luis and L. Vigara, *J. Org. Chem.*, 2009, **74**, 6130; (*c*) M. I. Burguete, F. Galindo, S. V. Luis and L. Vigara, *J. Photochem. Photobiol., A*, 2010, **209**, 61.

12 (*a*) I. Alfonso, M. I. Burguete and S. V. Luis, *J. Org. Chem.*, 2006, **71**, 2242; (*b*) I. Alfonso, M. I. Burguete, F. Galindo, S. V. Luis and L. Vigara, *J. Org. Chem.*, 2007, **72**, 7947.

13 (*a*) F. Adrián, M. I. Burguete, J. M. Fraile, J. I. García, E. García-España, S. V. Luis, J. A. Mayoral, A. J. Royo and M. C. Sánchez, *Eur. J. Inorg. Chem.*, 1999, 2347; (*b*) B. Altava, M. I. Burguete, N. Carbó, J. Escorihuela and S. V. Luis, *Tetrahedron: Asymmetry*, 2010, **21**, 982.

14 (*a*) I. Alfonso, M. Bolte, M. Bru, M. I. Burguete and S. V. Luis, *CrystEngComm*, 2009, **11**, 735; (*b*) I. Alfonso, M. Bru, M. I. Burguete, E. García-Verdugo and S. V. Luis, *Chem.–Eur. J.*, 2010, **16**, 1246.

15 S. Blasco, M. I. Burguete, M. P. Clares, E. García-España, J. Escorihuela and S. V. Luis, *Inorg. Chem.*, 2010, **490**, 7841.

16 (*a*) A. Andrés, C. Bazzicalupi, A. Bianchi, E. García-España, S. V. Luis, J. F. Miravet and J. A. Ramírez, *J. Chem. Soc. Dalton Trans.*, 1994, 2995; (*b*) M. Chadim, M. Budesinsky, J. Hodacova and J. Zavada, *Collect. Czech. Chem. Commun.*, 2000, **65**, 99; (*c*) M. Chadim, P. Díaz, E. García-España, J. Hodacova, P. C. Junk, J. Latorre, J. M. Llinares, C. Soriano and J. Zavada, *New J. Chem.*, 2003, **27**, 1132.

17 A. Bianchi, B. Escuder, E. García-España, S. V. Luis, V. Marcelino, J. F. Miravet and J. A. Ramirez, *J. Chem. Soc., Perkin Trans. 2*, 1994, **2**, 1253; J. A. Aguilar, E. García-España, J. A. Guerrero, S. V. Luis, J. M. Llinares, J. F. Miravet, J. A. Ramírez and C. Soriano, *Inorg. Chim. Acta*, 1996, **246**, 287; M. A. Bernardo, J. A. Guerrero, E. García-España, S. V. Luis, J. M. Llinares, F. Pina, J. A. Ramirez and C. Soriano, *J. Chem. Soc., Perkin Trans 2*, 1996, 2335; V. J. Arán, M. Kumar, J. Molina, L. Lamarque, P. Navarro, E. García-España, J. A. Ramírez, S. V. Luis and B. Escuder, *J. Org. Chem.*, 1999, **64**, 6135.

18 (*a*) S. P. Dagnall, D. N. Hague and M. E. J. McAdam, *J. Chem. Soc., Perkin Trans 2*, 1984, 435; (*b*) L. Alderighi, A. Bianchi, L. Biondi, L. Calabi, M. De Miranda, P. Gans, S. Ghelli, P. Losi, L. Paleari, A. Sabatini and A. J. Vacca, *J. Chem. Soc., Perkin Trans. 2*, 1999, 2741; (*c*) A. Bencini, A. Bianchi, E. García-España, M. Micheloni and J. A. Ramírez, *Coord. Chem. Rev.*, 1999, **188**, 97; (*d*) J. Aguilar, P. Díaz, F. Escartí, E. García-España, L. Gil, C. Soriano and B. Verdejo, *Inorg. Chim. Acta*, 2002, **39**, 307; (*e*) M. T. Albelda, J. C. Frias and E. García-España, *Encycl. Supramol. Chem.*, 2007, **1:1**, 1–37.

19 R. M. C. Dawson, *et al.*, *Data for Biochemical Research*, Clarendon Press, Oxford, 1959.

20 K. Sun Bai and A. E. Martell, *J. Am. Chem. Soc.*, 1969, **91**, 4412.

21 J. C. Stephens, M. A. Khan and R. P. Houser, *Inorg. Chem.*, 2001, **40**, 5064.

22 (*a*) T. R. Wagler, Y. Fang and C. J. Burrows, *J. Org. Chem.*, 1989, **54**, 1584; (*b*) B. Dangel, M. Clarke, J. Haley, D. Sames and R. Polt, *J. Am. Chem. Soc.*, 1997, **119**, 10865; (*c*) C. L. Weeks, P. Turner, R. R. Fenton and P. A. Lay, *J. Chem. Soc., Dalton Trans.*, 2002, 931; (*d*) M. I. Burguete, F. Galindo, S. V. Luis and L. Vigara, *Dalton Trans.*, 2007, 4027; (*e*) S. K. Sharma, S. Upreti and R. Gupta, *Eur. J. Inorg. Chem.*, 2007, 3247; (*f*) J. Singh, G. Hundal and R. Gupta, *Eur. J. Inorg. Chem.*, 2008, 2052; (*g*) R. Shakya, A. Jozwiuk, D. R. Powell and R. P. Houser, *Inorg. Chem.*, 2009, **48**, 4083.

23 (*a*) R. Polt, B. D. Kelly, B. D. Dangel, U. B. Tadikonda, R. E. Ross, A. M. Raitsimring and A. V. Astashkin, *Inorg. Chem.*, 2003, **42**, 566; (*b*) S. Autzen, H.-G. Korth, R. Boese, H. De Groot and R. Sustmann, *Eur. J. Inorg. Chem.*, 2003, 1401–1410; (*c*) A. G. Algarra, M. G. Basallote, C. E. Castillo, M. P. Clares, A. Ferrer, E. García-España, J. M. Llinares, M. A. Máñez and C. Soriano, *Inorg. Chem.*, 2009, **48**, 902.

24 (*a*) M. Kodama and E. J. Kimura, *J. Chem Soc., Dalton Trans.*, 1980, **17**, 839; (*b*) R. J. Motekaitis, B. E. Rogers, D. E. Reichert, A. E. Martell and M. J. Welch, *Inorg. Chem.*, 1996, **35**, 3821.

25 (*a*) K. Schug, P. Fryčák, N. M. Maier and W. Lindner, *Anal. Chem.*, 2005, **77**, 3660; (*b*) A. Di Tullio, S. Reale and F. J. De Angelis, *Mass Spectrom.*, 2005, **40**, 845; (*c*) B. Baytekin, H. T. Baytekin and T. C. A. Schalley, *Org. Biomol. Chem.*, 2006, **4**, 2825.

26 M. Munjal, S. Kumar, S. K. Sharma and R. Gupta, *Inorg. Chim. Acta*, 2011, **377**, 144.

27 (*a*) E. García-España, M.-J. Ballester, F. Lloret, J. M. Moratal, J. Faus and A. Bianchi, *J. Chem. Soc., Dalton Trans.*, 1988, 101; (*b*) M. I. Burguete, E. García-España, L. López-Diago, S. V. Luis, J. F. Miravet and D. Sroczynski, *Org. Biomol. Chem.*, 2007, **5**, 1935.

28 P. Gans, A. Sabatini and A. Vacca, *Talanta*, 1996, **43**, 1739.

29 L. Alderighi, P. Gans, A. Ienco, D. Peters, A. Sabatini and A. Vacca, *Coord. Chem. Rev.*, 1999, **184**, 311.

30 (*a*) P. K. Glasoe and F. A. Long, *J. Phys. Chem.*, 1960, **64**, 188; (*b*) A. K. Covington, M. Paabo, R. A. Robinson and R. G. Bates, *Anal. Chem.*, 1968, **40**, 700.

31 *SAINT, 5.0 ed*, Bruker Analytical X-Ray Systems, Madison, WI, 1996.

32 G. M. Sheldrick, *SHELXTL; 5.1 ed*, Bruker Analytical X-Ray Systems, Madison, WI, 1997.

33 L. J. Farrugia, *WinGX version 1.64, An Integrated System of Windows Programs for the Solution, Refinement and Analysis of Single-Crystal X-ray Diffraction Data*, Department of Chemistry, University of Glasgow, 2003.

34 *DIAMOND version 2.1c, Crystal Impact GbR*, Bonn, Germany, 1999.

